Revisiting fluorescein and layered double hydroxide using a synergistic approach: A complete optical study

Paul Legentil, Fabrice Leroux, Sandrine Therias, Rachid Mahiou, Geneviève Chadeyron

Revisiting Fluorescein and layered double hydroxide using a synergistic approach: a complete optical study

Paul Legentil, Fabrice Leroux, Sandrine Thérias, Rachid Mahiou and Geneviève Chadeyron*

Université Clermont Auvergne, Institut de Chimie de Clermont-Ferrand, UMR CNRS 6296, BP 10448, F-63000 Clermont-Ferrand, France

Abstract

The luminescence of Fluorescein, an inexpensive dye, ought to be interesting for lighting application devices such as commercial LEDs. However, the molecule suffers from severe instability, making it inappropriate for such applications. As previously studied, fluorescein molecules may be hosted in a layered double hydroxide (LDH), and the role of such an inorganic material in stabilizing the dye has been underlined. However, a deep understanding of the resulting optical properties is still required. Using extremely small amounts of fluorescein, it is demonstrated here that Zn_2Al cation-based LDH tethering acts as a «solid solvent» for the dye, enabling its luminescence even in powder form, whereas fluorescein molecules on their own emit no luminescence at all in the solid state. However, aggregations of the dye occur in the interlamellar space, leading to non-radiative emission. Emission and excitation spectra, as well as fluorescence decays, are studied to explain the difference between the hybrid LDH-Fluorescein material and an aqueous solution of fluorescein. Additionally, LDH platelets are found to help the dispersion of the intercalated fluorescein in silicone to obtain a homogeneous composite film, which exhibits luminescent properties. Finally, an accelerated photoaging study demonstrates that the LDH-fluorescein filler has a pro-degradant effect on polymer aging under UV radiation.

1. Introduction

In recent years, global warming on Earth has been causing major environmental problems. To respond to this growing concern, scientists orient their research towards sustainable solutions, and develop processes to save energy. Almost 20 % of the electricity consumption in the world is due to the lighting sector, explaining why light-emitting diodes (LED) have emerged to provide efficient and sustainable products replacing common lighting devices such as incandescent bulbs. However, commercial LEDs are manufactured using rare earth-based phosphors; these elements are expensive and not eco-friendly due to their extraction process and their life-cycle assessment. They might be replaced by organic fluorescent molecules that are cheaply available and sustainable. Even if these molecules exhibit high photoluminescent quantum yields, they nevertheless suffer from a lack of robustness in standard operating conditions, thus greatly limiting them as efficient phosphors in marketed lighting devices.

Fluorescein is a very common organic dye which has met with great interest for many years in a wide range of applications thanks to its biocompatibility, high molar absorptivity and excellent fluorescence quantum yield [1].

Fluorescein is an organic molecule belonging to the xanthene family and is used as a probe in medical and biological applications (optical imaging, detection of analytes…) [2-4]. Fluorescein is a red powder in the solid state, emitting a strong yellow-green light in liquid solution (in water at basic pH or ethanol for example) at low concentration (below 10^{-3} M) and under UV-blue excitation. At higher concentrations, a quenching phenomenon appears to reduce its light emission, and the solid powder does not luminesce at all. In solution, the dye can take several prototropic forms depending on the pH [5]. The dianionic form is the most luminescent one, and its contribution to the dye total

emission exceeds the others. A shoulder on the edge of the main peak (emission of the dianionic form) may be observed, indicating the presence of the monoanionic form [6]. Indeed, the monoanionic form also exhibits luminescent properties but its emission is much weaker, and the global emission spectra are blue-shifted with a broadening of the emission band compared to that of the dianionic form.

The optical properties of fluorescein could also lead to an interesting future in lighting applications, and particularly in the LED-based field. Indeed, fluorescein emits green-yellow radiation under blue excitation ($\lambda_{max\ exc}$ = 490 nm) compatible with a blue LED chip to produce a modulable (warm or cold) white light emission for lighting applications. Some studies [1, 7] have already emphasized the potential of fluorescein to replace phosphors associated with blue LEDs in commercial devices such as rare-earth based common YAG:Ce. However fluorescein, like organic molecules, is very sensitive to external photonic and thermal stress, and its luminescence quickly breaks down in use [8], which has so far been a limiting factor for further development.

To overcome this issue, one alternative is to protect the dye from quenching and instability (i.e. avoiding aggregation, thermal degradation, and so on) using a solid inorganic matrix, such as for example using Layered Double Hydroxides (LDH), an anion host structure. Recently, photoactive molecules intercalated into LDH layers have drawn much attention for the development of nanophotosensitizers for therapeutic uses [9], stimuli-responsive intelligent materials and luminescent sensors [10, 11]. Some studies [12] reported the intercalation of fluorescein molecules into LDH. These materials present an interest, especially for catalysis and environmental applications [13-15]. Their general chemical formula is: $[M(II)_{1-x}M(III)_x(OH)_2]^{x+}[A^{n-}]_{x/n}\cdot mH_2O$ where M(II) is a bivalent cation such as Zn^{2+}, Mg^{2+}, Fe^{2+}, etc.; M(III) is a trivalent cation such as Al^{3+}, Fe^{3+}, etc. and A^{n-} is an anion. The structure is layered and therefore anisotropic, built from cations and hydroxides having a net positive charge caused by the partial substitution of bivalent cations by trivalent cations. To ensure electroneutrality, anions are located in the interlayer space of the LDH with the presence of water molecules. Since the Fluorescein molecule is an anionic dye, it may be hosted within the LDH structure. The idea here is to possibly tether and stabilize fluorescein molecules while optimizing their luminescence properties. It also allows fluorescein to be isolated from the outside environment (O_2 from air) to avoid any accelerated oxidation and improve the dispersion of the fluorescein in a polymer to produce homogeneous composite films for LED-based devices. LDH-based fluorescent and phosphorescent thin films (TFs) elaborated by layer by layer (LBL) method have been reported in the literature [16-18]. Herein, we focused on self-supporting thin luminescent composite films LDH-Fluorescein/silicone which have been prepared by solution casting onto a Teflon surface using an Elcometer 4340 automatic film applicator. Indeed, from the point of view of the organic dye, LDH inorganic filler can be viewed as an anti-aggregation and protective agent, while from the LDH side, the dye appears as an organo-compatibilizing agent to better resist polymer dispersion.

In this paper, the synthesis and characterization of a hybrid LDH-Fluorescein (LDH-F) material are presented, and its optical properties are thoroughly examined. Among the several LDH, the Zn-Al host matrix was chosen for this study as it displays a higher crystallinity compared to the more usual hydrotalcite Mg-Al for example, thus allowing a more accurate characterization by XRD of the hybrid materials as well as the filler upon polymer dispersion. LDH was used as host matrix to prevent aggregation of fluorescein dye, allowing to avoid the quenching of the luminescence and acting as a protective environment. Indeed, the usual passive LDH filler becomes here a photofunctional active filler. The LDH matrix creates a dilute environment for the dye that is normally observed in an aqueous solution: the LDH provides the fluorescein molecules with an environment which is suitable for them to luminesce well. Although, several studies [19-21] about nanohybrids LDH-Fluorescein have been reported for different applications a complete understanding of the mechanisms involved is scarcely reported so far. In this work, the optical properties were deeply investigated and a better understanding is highlighted to unravel mechanisms responsible of the luminescence of the solid

powder LDH-F. Indeed, a better understanding permits here the mechanisms responsible for the luminescence to be identified**.** It is also demonstrated from an analysis of the photostability that LDH platelets stabilize the dye under potential operating conditions.

2. Experimental section

2.1. Materials

The two-component silicon polymer, Bluesil RTV 141 part A and part B, was supplied by Elkem. $Zn(NO_3)_2$.$6H_2O$ (purity 99.9+%), $Al(NO_3)_3$.$9H_2O$ (purity 99.9+%) and NaOH (97%) were obtained from Sigma Aldrich. The fluorescein disodium salt $C_{20}H_{10}Na_2O_5$ was purchased from Alfa Aesar.

2.2. Synthesis procedure of LDH hybrid materials using the coprecipitation method

The fluorescein layered double hydroxide phase, Zn_2Al– F, was prepared by the coprecipitation method with different fluorescein concentrations. The synthesis of $[Zn_2Al_1(OH)_6]^+[NO_3^-]_{1-x}[F^{2-}]_x{\cdot}mH_2O$ was performed using fluorescein disodium salt in 50 mL of de-ionized water. 50 mL of an aqueous solution of Zn^{2+} ($3.4x10^{-2}$ M) and Al^{+3} ($1.7x10^{-2}$ M) was added dropwise over a period of 3 hours under magnetic stirring. For instance, to make the $[Zn_2Al_1(OH)_6]^+[NO_3^-]_{0.999}[F^{2-}]_{0.0005}{\cdot}mH_2O$ sample, $5.2x10^{-1}$ mmol of fluorescein disodium salt was used.

The pH was maintained at 10.5 by adding 0.25 M NaOH during the synthesis processes. Coprecipitation was performed under nitrogen at 20°C. The mixture was centrifuged at 5,000 rpm for 5 minutes; the sedimented solid on the bottom of the flask was washed several times with de-ionized water until a clear and transparent supernatant was obtained. A paste was recovered and stored at 5°C. A small amount was dried overnight at room temperature to obtain a powder and to determine the proportion of the dry extract.

2.3. Elaboration of Silicone/HDL-F resin composite films

The LDH-F (0.05 %) powder or the similar paste was used to elaborate the polymer/hybrid composite material with different loadings. The two-component silicone polymer (silicone Bluesil-RTV 141 A&B) was composed of a viscous liquid, called part A, cured by a polyaddition reaction with a catalyser, part B.

The silicone film was prepared as follows: a mixture of part A and 10 phr of part B was prepared, homogenised with a mechanical mixer (Planetary Centrifugal vacuum Mixer “Thinky Mixer”) for 10 minutes at 500 rpm. Next, the final composite film was prepared by casting onto a Teflon surface using an Elcometer 4340 automatic film applicator. The knife blade height was set at 200 µm and the casting speed was 30 mm/s. This two-component silicone polymer was cured at 80°C for 2 hours. The film thickness was measured using an Elcometer 456 coating thickness gauge.

The preparation and the curing process for the composite films were the same as for the silicone film.

2.4. Characterisation

2.4.1. X-ray diffraction

LDH powders were characterised by X-Ray Diffraction; the patterns were measured with a Philips X-Pert Pro diffractometer operating with Cu-Kα radiation (λ=1.5418 Å). The data were collected in a 2θ range of between 5° and 70° with a step size of 1°/min.

2.4.2. Elemental analyses CHNS

Elemental analyses of LDH powders LDH-F were performed to determine the composition of samples with a Flash 2000 CHNS analyzers (Thermo Electron).

2.4.3. Thermogravimetric analysis

Thermogravimetric (TG) analysis were performed on a Setaram TGA 92 instrument with a linear heating rate of 5 °C.min^{-1} under air.

2.4.4. Fourier-transformed infrared spectroscopy

The infrared spectra were recorded using a Nicolet 5700-FTIR spectrometer with Omnic software. Spectra were obtained using a summation of 32 scans and a resolution of 4 cm^{-1}. LDH and fluorescein powders were studied using the KBr pellet technique.

In the case of silicone/LDH-F composite films, calibration of the thickness of the non-photodegraded samples was performed by normalising the absorbance at 2140 cm^{-1} in IR spectra, which corresponds to a vibration band of the (Si–H) bending mode relative to the silicone. All the spectra were compared with an absorbance of 0.240 at 2140cm^{-1}.

2.4.5. UV-Visible absorption

The UV–visible absorption spectra of the samples were recorded in the wavelength range of 200 to 800 nm with a UV–vis spectrophotometer (SP-3000 Plus) equipped with an integrating sphere and UV-Probe software.

2.4.6. Luminescence

Quantum yield efficiencies were measured using a C9920−02G PL-QY integrating sphere measurement system from Hamamatsu Photonics. The setup consisted of a 150 W monochromatized Xe lamp, an integrating sphere (Spectralon coating, ⌀= 3.3 in.) and a high-sensitivity CCD camera. Excitation and blue-excited emission spectra were recorded with a Jobin-Yvon apparatus consisting of a Xe lamp operating at 400 W coupled with two monochromators (Triax 550 and Triax 180) and a cryogenically cooled charge-coupled device (CCD) camera (Jobin–Yvon Symphony LN2 series) for emission spectra and Hamamatsu 980 photomultiplicator for excitation spectra. Excitation spectra were corrected for instrument response and Xe lamp intensity using sodium salicylate. The resolution of the system was better than 0.1 nm in both emission and excitation configurations. Luminescence decays were recorded using second-harmonic generation on a pulsed Nd:YAG OPO Ekspla NT342A laser (3–5 ns pulse duration, 10 Hz, 5 cm^{-1} line width, 0.3 mJ- 20 mJ in the UV-blue). The emitted photons were detected at right angles to the excitation and analyzed via an Edinburgh FLS980 spectrometer (Czerny-Turner monochromator, 300 mm focal length, 1200 grooves mm^{-1} grating and minimum pass band of 0.1 nm) equipped with Hamamatsu R928P PMT (200–850 nm range).

2.4.7. Scanning electron microscopy (SEM)

Scanning electron microscopy was performed with a ZEISS Supra 55 VP scanning electron microscope in high vacuum at 20 kV using a back-scatter electron detector (QBSD).

2.5. Irradiation of films

Polymer and composite photodegradation under artificial aging conditions was performed in a SEPAP 12-24 unit (ATLAS) by UV-visible light irradiation (λ>300 nm) in presence of oxygen at 60°C (controlled by a Pt thermocouple). The device comprised four medium-pressure mercury lamps (Novalamp RVC 400W) situated vertically at each corner of the chamber. The samples were placed

on a rotating carousel positioned in the centre of the chamber. Wavelengths below 300 nm were filtered by the glass envelope of the lamps.

3. Results and discussion

3.1. XRD characterisation

3.1.1. Diffractogram results

Figure 1 shows the XRD patterns of LDH-fluorescein powders synthetized by coprecipitation. The XRD patterns are shown as a function of the fluorescein relative input. The latter is expressed by the mole ratio between fluorescein and Al^{3+} cations used during coprecipitation. Diffraction planes (00ℓ) are the fingerprints of the layered structure of LDH [22]. For the sample with the least amount of fluorescein (a), the positions of 2θ = 10.1° and 20.2° (i.e. 0.78 nm and 0.39 nm) are characteristic of a nitrate LDH phase, and assigned to diffraction planes (003) and (006), respectively. As the amount of fluorescein increases, these peaks at 10.1° and 20.2° progressively disappear, and a series of harmonic peaks is shifted to a lower angle and located at 5.5°, 11°, 16.5°, and 22° for the sample with the highest fluorescein content. For the intermediate contents (fig. 1b, 1c, 1d and 1e), the XRD patterns overlapped and correspond to a combination of nitrate and fluorescein phases which are mixed. These XRD peaks can be integrated to calculate the amount of fluorescein present in the interlayer space (inset fig 1). A simple methodology based on pole concentration is used here. Indeed, for sample (h), the experimental XRD pattern does not show the nitrate signal, and the ratio of the integration of the first and second harmonics (003)/(006) of the fluorescein signals can be calculated, resulting in a constant $R^{Fluo}_{(003)/(006)}$. For other samples for which a combination of nitrate and fluorescein is observed, the (006) peak of the fluorescein signal merges with the (003) peak of the nitrate signal. Using the constant $R^{Fluo}_{(003)/(006)}$ and the integration of the merged signals, the ratio $(003)_{Fluo}/(003)_{nitrate}$ may be calculated for all the samples studied. These results are shown in the inset in figure 1.

For the series of harmonic peaks, the one at 2θ = 5.5° leads to a basal spacing of 1.61 nm and is ascribed to diffraction plane (003), such values agreeing well with the basal spacing observed for fluorescein intercalated between LDH layers according to either Costantino et al. [23] or Tanaka et al. [24]. Indeed, Costantino et al. showed that fluorescein can be intercalated in a Zn_2Al LDH matrix by the ion-exchange method from a LDH-perchlorate in a fluorescein solution. As in the present study, several concentrations of fluorescein were used, resulting in the presence of a pristine LDH phase with a fluorescein LDH phase exhibiting a basal spacing of 1.65 nm. A slightly lower value of 1.58 nm is observed for MgAl LDH. In this case and similarly to the present study, Tanaka et al. performed fluorescein intercalation by coprecipitation and reported the setting up of two distinct fluorescein phases depending on the pH of the synthesis, leading to two interlayer distances of 0.78 and 1.58 nm. According to Tanaka et al., guest accommodation within the interlayer domain for the former is horizontal to the inorganic sheets, while it is vertical (perpendicularly tilted) for the latter.

Elemental analysis of powders was performed for some samples (sample a, d and h) to determine the experimental fluorescein amounts remaining in the LDH powders after the synthesis. Microanalyses CHNS allows to find the mass fraction of C, N and H elements contained in each sample. Elemental analyses results are reported in table 1. Carbonate pollution in interlamellar space is likely as XRD patterns shown and has been taken into account in the calculations. Thus, the experimental formula can be easily calculated by using the experimental molecular mass Mw determined with thermogravimetric analysis (see fig. S1 in the Supporting Information). For instance, the experimental formula of the sample d obtained is: $Zn_2^{2+}Al^{3+}(OH^-)_6\ (CO_3^{2-})_{0.26}(NO_3^-)_{0.22}(Fluo^{2-})_{0.13}$,

1.5 H_2O in making assumption that the ratio Zn/Al = 2 is fixed, in this way x = 0.13 for fluorescein amount whereas the theoretical value expected was x = 0.15. In the same way, experimental formula for sample h is $Zn_2^{2+}Al^{3+}(OH^-)_6\ (CO_3^{2-})_{0.09}(NO_3^-)_{0.0.06}(Fluo^{2-})_{0.38}$, 2.8 H_2O whereas theoretical amount of fluorescein was x = 0.5. The experimental calculations were distorted when the amount of fluorescein was too weak (for the sample a) otherwise the experimental values are closed from the theoretical values. Thus, the coprecipitation method for intercalation fluorescein is well effective.

3.1.2. XRD interpretation of fluorescein intercalation

From the above interpretations, the attribution of the former value to an intercalated fluorescein LDH phase is questionable, since it corresponds to the basal spacing of the nitrate form. Tanaka et al. argued that the amount of fluorescein was 16.5 % of the total interleaved anions and that the amount of fluorescein adsorbed onto LDH carbonate platelets represented only 2.70 %. However, it is known [25] that carbonate anions present a high affinity towards the LDH framework and that they are not easily displaced unless acidic conditions or calcination are employed. Although Costantino et al. also worked with different concentrations of fluorescein, only one unique basal spacing of 1.65 nm was observed, although the pH of the ion-exchange reaction was the same (pH = 8) as the one for which Tanaka et al. observed a horizontal distribution of the fluorescein molecules with a basal spacing of 0.78 nm. The interpretation of Tanaka et al. is also in discrepancy with the present results, showing a unique stacked structure for a fluorescein loading of 10 %, which is comparable to some extent to the Tanaka et al. experimental conditions. It is interesting to note that for the low fluorescein content, the nitrate phase is observed. However, for a loading of 10 % fluorescein, a carbonate phase is clearly evidenced by the saw-toothed structure around 60° and attributed to diffraction peaks (110) and (103). Interestingly, carbonates anions displaced the initially interleaved anions when the interlayered gap was not fully occupied by the same anions (b, c and d), making some possible paths available within the interlayer space for the carbonate anions to diffuse.

To conclude this structural discussion, the basal spacing at 0.78 nm is characteristic of the nitrate LDH phase, and does not correspond to horizontally accommodated fluorescein molecules, since the space available, 0.30 nm (knowing that the thickness of the LDH cationic sheets is 0.48 nm), is too small for the cumbersome guest molecule and the not strictly planar fluorescein molecule (Figure 2) to be correctly lodged in the interlamellar space; this in addition to the low charge matching, which is not reasonably in favour of such a horizontal accommodation.

3.2. Luminescence properties

3.2.1. Emission spectra interpretation

Fluorescein powder does not exhibit luminescence properties; while in aqueous media the fluorescein dye is characterized by a bright yellow-green emission under blue excitation (fig. 3a) [5, 26, 27]. As shown in Fig 3b and c, a yellow green emission is recorded for HDL/fluorescein powder upon excitation at 450 nm, which is the wavelength corresponding to the emission of a commercial blue LED for a potential further association.

Fluorescence emission studies were undertaken using an excitation wavelength of 450 nm (corresponding to the emission of a commercial blue LED). The emission spectra of LDH-fluorescein (0.05 %, 1.25 % and 35%) powders are shown in fig. 3c. For comparison, the emission spectrum of fluorescein in aqueous solution (10^{-7} M, pH 10) has been added (fig. 3a). As the amount of fluorescein in the LDH phase increases, fluorescence intensity decreases and the spectra show a gradual red shift (fig. 3c). A high concentration of fluorescein in the LDH phase leads to a luminescence quenching

phenomenon (as seen in fig. 3c). The emission spectrum of the 0.05% LDH-Fluorescein sample shows a predominant peak at 520 nm with a shoulder at 556 nm. A similar trend in the emission spectrum is observed for fluorescein in diluted solution (fig. 3a). As described by De et al. [26, 28] the main emission is ascribed to the dianion while the shoulder contains several contributions, arising from the emission of some species due to a neutral form of the dye or some dye aggregates. The deconvolution of the broad emission band by Gaussian functions (fig. 3a and b) defines three contributions, both for the fluorescein in solution and for the LDH-F powder. However, as shown in table 2, the position and the intensity of each contribution are slightly different for the two samples, which can be explained by a change in the environment of the fluorescein dye. Each contribution could be ascribed to three different fluorescent species. Thus, based on previous work, we can consider that fluorescein luminesces through three forms which can be attributed, for the aqueous solution, to the dianionic form as well as the monoanionic and the neutral forms [28]. In this case, the dianionic form is the most luminescent form (red curve/solid line in fig. 3a), whereas the monoanionic form (green curve/dashed line in fig. 3a) and the neutral form (blue curve/dash-dot line) are red-shifted with a lower intensity. For the LDH-F sample, the green (dashed line) contribution intensity becomes higher than the red one (solid line) indicating that the monoanionic population is higher than the dianionic population. This result can be explained by introducing the concept of "aggregates". Aggregation depends on many parameters, such as the structure of the monomer but also the nature of the solvent (if the environment is liquid), temperature, pH values and ionic strength. According to the Kasha and El-Bayoumi report [29], several absorption peaks are observed in a solution containing aggregates. A monomer molecule has a singlet excited state, while a dimer will have two levels: one with lower energy than the monomer singlet excited state and one at higher energy, according to the molecular exciton model. Figure 4 illustrates the mechanism resulting from the aggregation of two single fluorescein molecules. Depending on the orientation of the molecules in the aggregate, one of these levels will be a permitted absorption transition, which will be forbidden for the others. For a dye such as fluorescein, which belongs to the xanthene family, aggregation is due to conjugated rings through the π-stacking effect. When dipoles of each molecule are arranged in a parallel manner (fig. 4a), only the transition to the higher energy level is allowed, and hence the electronic absorption transition in the dimer will be blue-shifted in comparison to the monomer [30]. For aggregates in which the monomers are arranged in a head-to-tail manner (fig. 4b), only a transition to the lowest split level is permitted. As a result, the emission spectrum is red-shifted with respect to the monomer. As mentioned by S. Das et al., the head to tail arrangement cannot be observed in LDH-F. Based on these results, the different contributions of the emission spectrum in figure 3b can be detailed as follows: the main emission peak can be assigned to the dianionic form (monomer), while the peak at the shorter wavelength can be attributed to the dianionic dimer arranged in a parallel manner, and the peak at the higher wavelength (590 nm) corresponds to the monoanionic monomer.

To examine the fluorescein environment close to LDH platelets, the excitation spectra were recorded and studied.

3.2.2. Excitation spectra

The excitation spectra of the LDH-F sample were recorded by monitoring three emission wavelengths (fig. 5). It appears that the excitation spectra depend strongly on the monitored emission wavelength. In any case, the excitation bands were located in the range lying between 375 and 530 nm and exhibited three contributions corresponding to the different arrangements of the fluorescein dye. As previously stated, we can easily attribute the band close to 490 nm to the dianionic form, and the shoulder around 475 nm to the monoanionic form of the fluorescein. The broad band located at 400 nm can be ascribed to another fluorescein form. Indeed, according to

Sjoback et al. [31] this excitation band may arise from dimers constituted of two aggregated monomers in parallel stacking. This assumption is in agreement with the findings of Kasha and El Bayoumi, who expected a blue-shifted band [21]. We also could not exclude the possibility that part of the fluorescein was adsorbed onto the surface of the LDH layers. To attempt to discard or retain this possibility, the excitation spectra of calcinated LDH-nitrate and LDH-carbonate with adsorbed fluorescein were recorded (fig. 5b and c, respectively). These samples were prepared from calcinated LDH-nitrate and LDH-carbonate dispersed in fluorescein solution (10^{-6} M). In these conditions, the fluorescein dye was only adsorbed at the surface of the oxide obtained by the calcination of the LDH or of the layers in the case of the LDH-carbonate. In the absence of any intercalation, the same behaviour was observed, meaning that the environment between intercalated and adsorbed fluorescein molecules in the LDH (fig. 5a) is similar. Stacking onto the platelets is surmised at this stage.

3.2.3. Luminescence Decays

All the excitation spectra shown in Fig.5 clearly exhibit three broad contributions peaking at around 400, 450 and 490 nm. The intensities of these bands differ from one sample to another, but remain quite constant in position when the monitored emission is modified. Selective excitation is difficult to elucidate, since the three contributions are close in position and overlapping. Considering the sample of interest (Fig.5a), the excitation at around 490 nm seems to be the most useful for an analysis of the dynamic processes. This position fits the absorption maximum observed for fluorescein in the xanthene major form in solution, as reported by Zhang et al. [32], which is around 496 nm. It is attributed to the $^1S_0 \rightarrow {}^1S_1$ absorption transition. The time decay of the fluorescein in solution is reported to be around 3-4 ns and must be measured using a high-frequency laser with ~ps pulse duration. These possibilities are not available with our measurement apparatus.

Despite this, luminescence decays can be recorded for the LDH-F sample, indicating that the LDH host modifies the decay time of the fluorescein since the time range of luminescence decays extends to the ms range, as observed in fig 6. To record the luminescence decays, three wavelengths were considered, one in the middle of the broad emission band at 535 nm and the two others on the high and low edge energy sides at 485 and 605 nm.

The deconvolution method was used to fit the decays by double exponential form, one in the rise and the second in the tail of the decays using the function $I(t)= A - B.\exp^{(-t/\tau 1)} + C.\exp^{(-t/\tau 2)}$, where A corresponds to the contribution of the noise and B and C are respectively the contributions of the rise and the long decay with the τ_1 and τ_2 time constants. The reliability of the fits is higher than 96%, the A contribution to the overall luminescence decays is less than $\sim 4.10^{-3}$ % and can be l considered as negligible. The derived τ_1 and τ_2 values are reported in table 3. All decays have the same shape and show no dependence on either emission or excitation wavelengths. We can state that the recorded luminescence, due to the long luminescence decay time, is inherently phosphorescent, arising from the triplet state of the fluorescein. Such consideration has been reported by D-J. Lougnot et al. [33] which have estimated that absorption-emission-decaying $^1S_0 \leftrightarrow {}^1S_1$ processes occur during the laser pulse when its duration is larger than the photoionization process. However, the transition emission arising from the $^3T_1$ state should be accompanied by a red shift for the emission. To the best of our knowledge, only one paper reports the position of the $^3T_1 \rightarrow {}^1S_0$ transition in the case of fluorescein, which lies at around 625 nm. Our measurements of the luminescence emissions show clearly that no such notable shift was observed between fluorescein in solution and that in LDH-F. Moreover, the luminescence decays of the fluorescein in solution exhibit the same shape than that of fluorescein intercalated in LDH.

Considering the decay results, the rise is always similar at around 700 ns. The nature of this rise was the subject of further experiments, notably by checking Time Resolved Spectroscopy. The long decay time constant is around 700 ns. The two values are similar, indicating that that the species present in the LDH-F are probably thermalized in terms of energy levels and exhibit mutual energy transfer. The increase in fluorescence lifetime in LDH-F compared to the reported results concerning fluorescein in solution is an indication that the photoluminescence quantum yield is reduced.

3.2.4. Absolute photoluminescence quantum yields

The absolute photoluminescence quantum yields (PL QY_{ab}) of LDH-F powder and paste samples with varying amounts of fluorescein (between 0.05% to 35% of the occupied interlamellar space) were recorded upon excitation in the 250-500 nm range, as shown in fig. 7. For all the samples (fig. 7a for powders and 7b for pastes), the PL QY_{ab} evolution as a function of the excitation wavelength, leads to the same profiles. The absolute quantum yield of the fluorescein in water-based solution of 10^{-4} mol. concentration, upon 450 nm excitation, is of about 65%. The emission spectrum of LDH-F (fig. 3b) is the same as the emission spectrum of fluorescein in solution (fig. 3a) under such excitation, indicating that the intercalation doesn't modify the main electronic structure of the emitting species. For the LDH-F the LDH layers to some extent confine the fluorescein molecules on the basis of host–guest interactions (such as ionic interactions), and the anionic state, molecular configuration and microenvironment of interlayer fluorescein may be totally different from the fluorescein solution.

The samples with a very small amount of fluorescein exhibit only photoluminescence properties. Indeed, the amount of fluorescein must be lower than 1 % in the LDH to record a PL QY_{ab} higher than 5% for either powder or paste. For both samples, the best PL QY_{ab} is reached for an excitation wavelength of 490 nm, corresponding to maximum fluorescein absorption. The maximum values of absolute quantum yield were measured for LDH-F (0.05 %) paste, with a value of 21.4 %. PL QY_{ab} is higher for the paste sample than for the powder, and two assumptions can be suggested. The first concerns the effect of water in the paste; indeed, the paste produced after centrifugation contains roughly 80 wt. % of water and 20 wt. % of powder. In this case, the fluorescein molecules are in an environment that is close to that of a solution, explaining why luminescence is increased. The second possibility relies on the reflective index (RI). The RI of water is 1.33, against 1 for air; thus, the paste which contains water will absorb more photons. Accordingly, absorption is greater for the paste and its PL QY_{ab} is improved.

The intercalation of fluorescein in such low concentrations (0.05 %) cannot be detected from XRD patterns, where only the nitrates are visible (as seen in fig. 1). Nevertheless, we can suppose, based on the emission and excitation spectra that the fluorescein molecules are in close proximity to the LDH, most probably adsorbed onto the LDH platelet surfaces.

We have demonstrated that the fluorescein dye must be present in the LDH in small quantities to provide luminescence properties. Such behaviour can be explained by a concentration quenching phenomenon, which is predominant when the concentration of fluorescein dye increases. When the fluorescein molecules are closed, they formed aggregates by π-stacking (parallel stacking) due to conjugated xanthene rings or by hydrogen bonding (head-to-tail) with carboxylic acid and alcohol groups [26]. Fluorescein is well-known [28] for self-quenching its luminescence when the concentration reaches a sufficiently high value to form these aggregates of monomer molecules such as dimers, trimers etc. Although the monomer exhibits good luminescence properties, all the aggregates led to an extinction of the optical properties due to non-radiative energy transfer between the dye molecules [34]. This phenomenon increases with the dye concentration in solution, and for fluorescein powder no luminescence is observed. As a conclusion, we have shown that the

lamellar space of the LDH host matrix can be considered as a dilution medium for the fluorescein dye, and plays the same dispersing role as that of an aqueous solution.

3.3. Composite film LDH-F/silicone

3.3.1. Luminescence properties

The LDH-F powder presenting the best absolute quantum yield efficiency value was used in this section. TEM (see fig. S2 in the Supporting Information) revealed that LDH-F powder consisted of pseudo-hexagonal nanosheets stacked on top of each other. The LDH-F (0.05 %) was dispersed in a silicone resin to prepare the composite films. The thickness of the composite films ranged from 100 to 120 µm. Composite film homogeneity as well as the random orientation dispersion of the LDH platelets has been shown by SEM (see fig. S3 in the Supporting Information)**.** In order to get a composite film suitable for a commercial blue LED, the LDH/dye nanohybrids were dispersed in a polymer such as silicone. The PL QY_{ab} of the composite films with variable amounts (between 10 % to 60 %) of LDH-F (0.05% powder), were recorded under excitation in the 250-500 nm range, as shown in fig. 8a. The best PL QYab was achieved on excitation at 490 nm for each composite film, and increased gradually with the quantity of LDH-F particles in the silicon matrix. This could be explained by an increase in the absorption of photons with the increase in filler loading. On the other hand, when the percentage of LDH-F particles was too high (> 40 wt. %), the mixture of powder and silicon became inhomogeneous and the composite films could not be hardened, due to excessive quantities of nanoparticles compared to the silicone resin. Thus, the percentage of LDH-F (0.05 %) particles dispersed within the silicone resin is fixed at 20 wt. % in the following. Moreover, the PL QY_{ab} recorded for the homogenous composite film elaborated with a loading of LDH-F of 40 wt. % (PL QY_{ab}=25%) is higher than that obtained for the powder and paste LDH-F (0.05 %) samples. The value of 25% for the PL QY_{ab} remains low for general lighting LED but could be of interest for other LED applications such as display and anticounterfeiting for example. We can also add that the silicone matrix enables the creation of a dilution medium for the LDH-F powder, thus improving its luminescent properties.

LDH platelets exhibit a good compatibility with the silicone matrix thereby providing a homogeneous dispersion. Previous studies demonstrated an efficient dispersion of organo-modified LDH within PDMS type polymer [35]. To confirm the interest of the LDH matrix in the dispersion of fluorescein in the silicone matrix, a composite (silicone/$fluorescein_{0.02\%}$) film was prepared. The amount of fluorescein therein was comparable to the amount of pure fluorescein contained in the composite silicone LDH-F (0.05 %) film with 20 wt. % of filler loading. This composite silicone/$fluorescein_{0.02\%}$ film emits no luminescence at all, as shown in figure 8a, thus confirming the action of LDH as a “solid solvent” in diluting the fluorescein, resulting in greater luminescent properties for the composite films. In this 2D organized structure, the fluorescein dye is intercalated in the interlayer gallery space. In this configuration, the fluorescein molecules are spaced away from each other and the quenching due to the aggregation is avoided.

The emission spectrum of the composite films is similar to that recorded for the powder. Indeed, as for the LDH-F (0.05 %) powder, the three contributions of fluorescein are observed (fig. 8b).

3.3.2. Photostability of LDH-F/silicone composite films

The photostability of the fluorescein chromophore dispersed into the composite films represents one of the key parameters for potential application in LED device. To the best of our

knowledge, this paper is the first study of the photostability of LDH-F/silicone composite films. Composite films with LDH-fluorescein and LDH-nitrate and pure silicone film were irradiated in accelerated ageing conditions (λ>300, 60°C) to study the potential effects that LDH and fluorescein could have on silicone photooxidation.

The chemical modifications during irradiation were monitored by IR spectroscopy. Fig. 9a presents the FTIR spectra of a pure silicone film (without filler) as a reference during irradiation under accelerated artificial conditions. The initial spectrum is typical of a silicon polymer like PDMS. The two intense bands at 2960 and 2075 cm^{-1} are relative to the (C-H) vibration mode of the silicone. The region between 1800 and 2200 cm^{-1} reveals IR bands corresponding to (Si-O) and (Si-H) vibration modes. The two bands near 1405 and 1445 cm^{-1} are ascribed to CH_3 symmetrical bending vibration. The IR spectrum of silicone during the aging process presents a decrease in two bands, one at 2140 cm^{-1} relative to the (Si-H) vibration mode and one at 905 cm^{-1} (Si-O-Si). In fig. 9b and c, both IR bands are shown after subtracting the spectra from the initial spectrum (t = 0). To distinguish the thermal curing effect from the photooxidation of the silicone polymer, a post-curing experiment was performed at 80°C for 264 hours on the composite films and the pure silicone film. FTIR spectra were then recorded before and after post-curing. Both FTIR spectra of the pure silicon film are presented in fig. 10. The IR spectrum after post-curing shows the decrease in absorbance of the two IR bands at 2140 cm^{-1} and 905 cm^{-1}. Thus, the modifications of these two bands are due to a post-curing phenomenon and not to a photooxidation process.

Fig. 11a shows the spectra of a silicone/LDH-F composite film during irradiation, and Figs 11b and c, present subtracted spectra. Before irradiation, the IR spectrum of the silicone/LDH-F composite film shows a broad and intense band around 3500-3600 cm^{-1}, assigned to the (O-H) stretching of water molecules and hydroxyl groups from the LDH matrix. At 1605 cm^{-1}, water from the LDH is observed, as well as the characteristic band at 1350 cm^{-1} of nitrate in LDH. The metal-oxygen vibrations of LDH can be noticed in the region of 1000-400 cm^{-1}. During irradiation, two IR bands are modified at 2140 cm^{-1} and 905 cm^{-1}, as observed in the case of the reference silicone film. Moreover, a new IR band at 1725 cm^{-1} develops upon irradiation for the silicone/LDH-F composite film. This new IR band can be ascribed to photodegradation products of the polymer matrix. The modification observed for the broad and intense band around 3500 cm^{-1} may be due to a change in the hydration of the samples during irradiation.

Variations in the absorbance of the IR bands at 2140 cm^{-1}, 1725 cm^{-1} and 905 cm^{-1} during irradiation were plotted as a function of time for the silicone film and both composite films, silicone/HDL-F (0.05%) and silicone/LDH-N (with nitrate ions intercalated), and are shown in Fig. 12. A decrease in absorbance for the two IR band at 2140 cm^{-1} and 905 cm^{-1} was observed for the three films (pure silicone and the two composite films with LDH-F and LDH-N), with approximately the same kinetic curves, due to a post-curing phenomenon.

At 1725 cm^{-1}, the same modification is observed during photoaging between the silicone/LDH-F composite and the composite film with LDH-N, both adopting a similar kinetic. The band at 1725 cm^{-1} in the pristine silicone film is also slightly visible (Fig. 9b). Thus, the formation of this IR band in the composite film could be explained by the photodegradation of the silicone polymer, where the presence of an LDH matrix (in both cases, LDH-F and LDH-N) has a pro-degradant effect.

These results show that in accelerated aging conditions, photodegradation of the silicone matrix is observed in presence of LDH, either with LDH-F or with LDH-N. This effect is not due to the presence of fluorescein molecules in the composite.

4. Conclusion

In this study, it has been demonstrated that fluorescein molecules could be intercalated in large amounts into an LDH host structure, adopting a vertical orientation. However, only extremely small amounts of fluorescein in the lamellar space enable a yellow luminescent powder to be obtained. Fluorescein accommodation is then not detected by XRD. Indeed, from the optical properties of the LDH-F hybrid material, several emission contributions relative to different species are explained by a model in which the dianionic monomer, the monoionic monomer and the dianionic dimer forms of the fluorescein coexist. Thus, LDH brings a “solid solvation effect” to the fluorescein. The LDH-F hybrid material can be dispersed in a polymer matrix such as silicone to yield a luminescent composite film. LDH enables a homogeneous film to be produced, which was not possible with fluorescein alone. From the point of view of the organic phosphor, LDH layers provide dispersion avoiding quenching and migration while for LDH, the dye supplies the photoactivity.

The dispersion of the LDF-F filler in the silicone matrix does not affect the optical properties of the hybrid material, the PLQY being even higher than for the powder. From the photoaging study, it has been shown that the presence of LDH-F or LDH-N filler modifies polymer photostability during irradiation, and that this is due to the presence of LDH platelets rather than being caused by the fluorescein molecules. Fluorescein was used as a model to study the added-value of hybrid materials based on a phosphor and an LDH host matrix. In this vein LDH host efficiently the organic phosphor. These results showed the potentiality of LDH as photofunctional active filler and this approach can be extended to other phosphors such as organic dyes or quantum dots.

Formatting of funding sources

This work was supported by CPER DEFI MMASYF through its 2016 «MetaProfile» project. Thus, the authors thank European Union in the framework of the European Regional Development Fund (ERDF), and Région Auvergne Rhône-Alpes, which co-funded this project.

References

[1] J.-Y. Jin, H.-G. Kim, C.-H. Hong, E.-K. Suh, Y.-S. Lee, White light emission from a blue LED, combined with a sodium salt of fluorescein dye, Synthetic Metals, 157 (2007) 138-141. https://doi.org/10.1016/j.synthmet.2007.01.008

[2] R.F. Spaide, J.M. Klancnik, Jr, M.J. Cooney, Retinal vascular layers imaged by fluorescein angiography and optical coherence tomography angiography, JAMA Ophthalmology, 133 (2015) 45-50. https://doi.org/10.1001/jamaophthalmol.2014.3616

[3] H. Komatsu, N. Iwasawa, D. Citterio, Y. Suzuki, T. Kubota, K. Tokuno, Y. Kitamura, K. Oka, K. Suzuki, Design and Synthesis of Highly Sensitive and Selective Fluorescein-Derived Magnesium Fluorescent Probes and Application to Intracellular 3D Mg2+ Imaging, Journal of the American Chemical Society, 126 (2004) 16353-16360. https://doi.org/10.1021/ja049624l

[4] A. Kaines, I. Tsui, D. Sarraf, S. Schwartz, The Use of Ultra Wide Field Fluorescein Angiography in Evaluation and Management of Uveitis, Seminars in Ophthalmology, 24 (2009) 19-24. https://doi.org/10.1080/08820530802520095

[5] N. Klonis, W.H. Sawyer, Spectral properties of the prototropic forms of fluorescein in aqueous solution, Journal of Fluorescence, 6 (1996) 147-157. https://doi.org/10.1007/bf00732054

[6] C.A.B. Rodrigues, C. Graça, E. Maçôas, A. Fedorov, C.A.M. Afonso, J.M.G. Martinho, Excited-State Proton Transfer of Fluorescein Anion as an Ionic Liquid Component, The Journal of Physical Chemistry B, 117 (2013) 14108-14114. https://doi.org/10.1021/jp408616r

[7] P. Uthirakumar, C.-H. Hong, E.-K. Suh, Y.-S. Lee, Yellow light-emitting polymer bearing fluorescein dye units: Photophysical property and application as luminescence converter of a hybrid LED,

536 Reactive and Functional Polymers, 67 (2007) 341-347.
537 https://doi.org/10.1016/j.reactfunctpolym.2007.01.012
538 [8] S.A. Smith, W.A. Pretorius, The conservative behaviour of fluorescein, Water SA, 28 (2002) 403-
539 406. https://doi.org/10.4314/wsa.v28i4.4913
540 [9] R. Gao, X. Mei, D. Yan, R. Liang, M. Wei, Nano-photosensitizer based on layered double hydroxide
541 and isophthalic acid for singlet oxygenation and photodynamic therapy, Nature Communications, 9
542 (2018) 2798. 10.1038/s41467-018-05223-3
543 [10] Y. Zhao, H. Lin, M. Chen, D. Yan, Niflumic Anion Intercalated Layered Double Hydroxides with
544 Mechano-Induced and Solvent-Responsive Luminescence, Industrial & Engineering Chemistry
545 Research, 53 (2014) 3140-3147. https://doi.org/10.1021/ie404054v
546 [11] R. Gao, D. Yan, Layered host–guest long-afterglow ultrathin nanosheets: high-efficiency
547 phosphorescence energy transfer at 2D confined interface, Chemical Science, 8 (2017) 590-599.
548 https://doi.org/10.1039/C6SC03515A
549 [12] J.H. Lee, D.Y. Jung, E. Kim, T.K. Ahn, Fluorescein dye intercalated layered double hydroxides for
550 chemically stabilized photoluminescent indicators on inorganic surfaces, Dalton transactions, 43
551 (2014) 8543-8548. https://doi.org/10.1039/c4dt00692e
552 [13] L. Yan, Y. Wang, J. Li, S. Kalytchuk, A.S. Susha, S.V. Kershaw, F. Yan, A.L. Rogach, X. Chen, Highly
553 luminescent covalently bonded layered double hydroxide–fluorescent dye nanohybrids, Journal of
554 Materials Chemistry C, 2 (2014) 4490. https://doi.org/10.1039/c3tc32483d
555 [14] E. Conterosito, I. Benesperi, V. Toson, D. Saccone, N. Barbero, L. Palin, C. Barolo, V. Gianotti, M.
556 Milanesio, High-Throughput Preparation of New Photoactive Nanocomposites, ChemSUSchem, 9
557 (2016) 1279-1289. https://doi.org/10.1002/cssc.201600325
558 [15] S.P. Lonkar, B. Kutlu, A. Leuteritz, G. Heinrich, Nanohybrids of phenolic antioxidant intercalated
559 into MgAl-layered double hydroxide clay, Applied Clay Science, 71 (2013) 8-14.
560 https://doi.org/10.1016/j.clay.2012.10.009
561 [16] D. Yan, J. Lu, L. Chen, S. Qin, J. Ma, M. Wei, D.G. Evans, X. Duan, A strategy to the ordered
562 assembly of functional small cations with layered double hydroxides for luminescent ultra-thin films,
563 Chemical communications, 46 (2010) 5912-5914. 10.1039/C0CC00522C
564 [17] R. Gao, D. Yan, Ordered assembly of hybrid room-temperature phosphorescence thin films
565 showing polarized emission and the sensing of VOCs, Chemical communications, 53 (2017) 5408-
566 5411. https://doi.org/10.1039/C7CC01794D
567 [18] R. Gao, D. Yan, D.G. Evans, X. Duan, Layer-by-layer assembly of long-afterglow self-supporting
568 thin films with dual-stimuli-responsive phosphorescence and antiforgery applications, Nano
569 Research, 10 (2017) 3606-3617. https://doi.org/10.1007/s12274-017-1571-x
570 [19] W. Shi, S. He, M. Wei, D.G. Evans, X. Duan, Optical pH Sensor with Rapid Response Based on a
571 Fluorescein-Intercalated Layered Double Hydroxide, Advanced Functional Materials, 20 (2010) 3856-
572 3863. https://doi.org/10.1002/adfm.201001081
573 [20] W. Shi, M. Wei, D.G. Evans, X. Duan, Tunable photoluminescence properties of fluorescein in a
574 layered double hydroxide matrix and its application in sensors, Journal of Materials Chemistry, 20
575 (2010) 3901-3909. 10.1039/B921290F
576 [21] W. Shi, Z. Sun, M. Wei, D.G. Evans, X. Duan, Tunable Photoluminescence Properties of
577 Fluorescein in a Layered Double Hydroxide Matrix by Changing the Interlayer Microenvironment, The
578 Journal of Physical Chemistry C, 114 (2010) 21070-21076. https://doi.org/10.1021/jp1069863
579 [22] S. Aisawa, S. Sasaki, S. Takahashi, H. Hirahara, H. Nakayama, E. Narita, Intercalation of amino
580 acids and oligopeptides into Zn–Al layered double hydroxide by coprecipitation reaction, Journal of
581 Physics and Chemistry of Solids, 67 (2006) 920-925. https://doi.org/10.1016/j.jpcs.2006.01.004
582 [23] U. Costantino, N. Coletti, M. Nocchetti, G.G. Aloisi, F. Elisei, L. Latterini, Surface Uptake and
583 Intercalation of Fluorescein Anions into Zn−Al−Hydrotalcite. Photophysical Characterization of
584 Materials Obtained, Langmuir, 16 (2000) 10351-10358. https://doi.org/10.1021/la001096d
585 [24] A.S. Tanaka M., Takahashi S., Natita E., Synthesis and cellular uptake of fluorescein intercalated
586 layered double hydroxide, The Clay Science Society of Japan, 14 (2010) 5.
587 https://doi.org/10.11362/jcssjclayscience.14.5_197

588 [25] T. Hibino, Acid Treatment of Layered Double Hydroxides Containing Carbonate, European
589 Journal of Inorganic Chemistry, 2014 (2014) 5311-5321. https://doi.org/10.1002/ejic.201402372
590 [26] S. De, S. Das, A. Girigoswami, Environmental effects on the aggregation of some xanthene dyes
591 used in lasers, Spectrochimica Acta Part A: Molecular and Biomolecular Spectroscopy, 61 (2005)
592 1821-1833. https://doi.org/10.1016/j.saa.2004.06.054
593 [27] N.N. Math, L.R. Naik, H.M. Suresh, S.R. Inamdar, Dual fluorescence and laser emissions from
594 fluorescein-Na and eosin-B, Journal of Luminescence, 121 (2006) 475-487.
595 https://doi.org/10.1016/j.jlumin.2005.11.013
596 [28] S. De, R. Kundu, Spectroscopic studies with fluorescein dye—Protonation, aggregation and
597 interaction with nanoparticles, Journal of Photochemistry and Photobiology A: Chemistry, 223 (2011)
598 71-81. https://doi.org/10.1016/j.jphotochem.2011.07.002
599 [29] M. Kasha, H. Rawls, M. Ashraf El-Bayoumi, The exciton model in molecular spectroscopy, in:
600 Pure and Applied Chemistry, 1965, pp. 371-392.
601 [30] A. Eisfeld, J.S. Briggs, The J- and H-bands of organic dye aggregates, Chemical Physics, 324 (2006)
602 376-384. https://doi.org/10.1016/j.chemphys.2005.11.015
603 [31] R. Sjöback, J. Nygren, M. Kubista, Absorption and fluorescence properties of fluorescein,
604 Spectrochimica Acta Part A: Molecular and Biomolecular Spectroscopy, 51 (1995) L7-L21.
605 https://doi.org/10.1016/0584-8539(95)01421-P
606 [32] X.-F. Zhang, J. Zhang, L. Liu, Fluorescence Properties of Twenty Fluorescein Derivatives: Lifetime,
607 Quantum Yield, Absorption and Emission Spectra, 24 (2014) 7. https://doi.org/10.1007/s10895-014-
608 1356-5
609 [33] D.J. Lougnot, C.R. Goldschmidt, Photoionization of fluorescein via excited triplet and singlet
610 states, Journal of Photochemistry 12 (1980) 9.
611 [34] S. Das, A.P. Chattopadhyay, S. De, Controlling J aggregation in fluorescein by bile salt hydrogels,
612 Journal of Photochemistry and Photobiology A: Chemistry, 197 (2008) 402-414.
613 https://doi.org/10.1016/j.jphotochem.2008.02.003
614 [35] J.F. Naime Filho, F. Leroux, V. Verney, J.B. Valim, Percolated non-Newtonian flow for silicone
615 obtained from exfoliated bioinorganic layered double hydroxide intercalated with amino acid,
616 Applied Clay Science, 55 (2012) 88-93. https://doi.org/10.1016/j.clay.2011.10.010

617

618

LDH sample	C (wt %)	N (wt %)	H (wt %)	Mw (g.mol $^{-1}$)
a	0.84	4.6	3.0	449.84
d	0.93	10.5	3.20	334.13
h	0.21	21.4	3.8	431.43

619 *Table 1 : Elemental analyses obtained from CHNS analysis and molecular mass obtained by TGA analysis of LDH samples a, d*
620 *and h.*

621

622

Emission spectra		λ_{max} (nm)	E (cm^{-1})	FMWH (cm^{-1})
Fluorescein in water (10^{-7} M)	Red contribution (dash)	514	19437	926
	Green contribution (dot)	535	18706	1453
	Blue contribution (dash-dot)	564	17736	2239
LDH-fluorescein (0.05%) powder	Red contribution (dash)	518	19288	1083
	Green contribution (dot)	545	18358	1707
	Blue contribution (dash-dot)	582	17171	2660

623 *Table 2 : Results of the emission bands deconvolution by the sum of three gaussian functions fig. 3a and b*

		Time constants		Fitting goodness
		τ_1 (ns)	τ_2 (ns)	Adjusted R^2
Emission wavelengths	485 nm	706	716	0.967
	535 nm	707	723	0.992
	605 nm	674	676	0.996

Table 3 : Time constants derived from the fitting of the experimental values of the LDH-F (0.05%) powder fluorescence lifetime decay monitored at three emission wavelengths

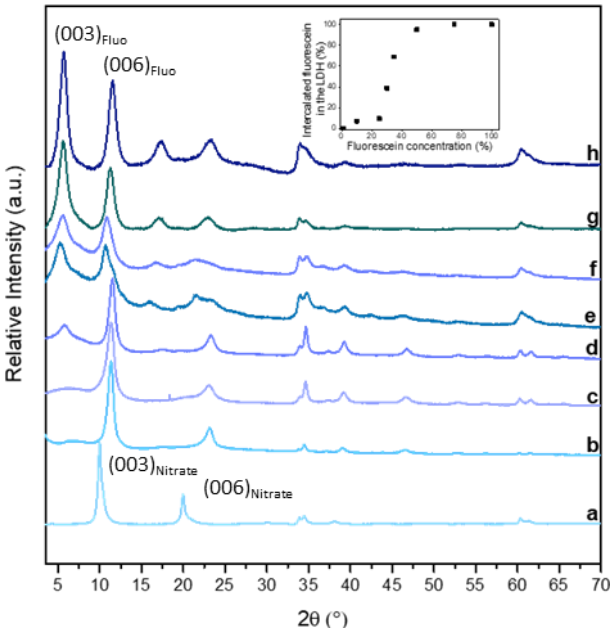

Figure 1 : X-Ray diffractograms of LDH-Fluorescein powder samples with different concentrations of fluorescein (a, b, c, d, e, f, g and h: 0.05%, 10%, 25%, 30%, 35%, 50%, 75% and 100%). Inset: Amount of intercalated fluorescein in LDH interlayer space in function of fluorescein concentration used in the XRD samples taking a and h as end-member of the nitrate vs fluorescein LDH substitution respectively.

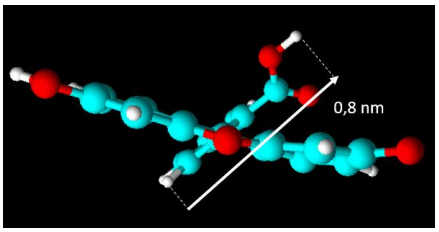

Figure 2 : Schematic representation of fluorescein seen from the xanthen frame plan

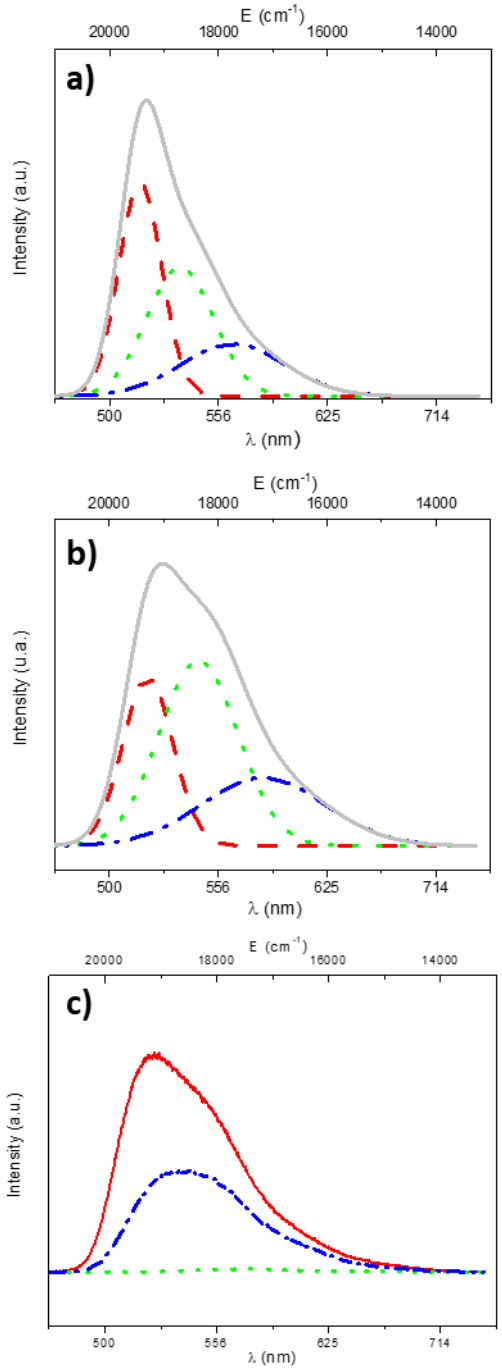

Figure 3: Emission spectra at 20°C with excitation at 450 nm of: a) fluorescein in water (10^{-7} M) with deconvolution in three contributions. b) LDH-fluorescein (0.05%) powder with deconvolution in three contributions. c) LDH-fluorescein powder with three loadings of fluorescein in LDH host (0.1 % —, 1.25 % – – – and 35% - - -)

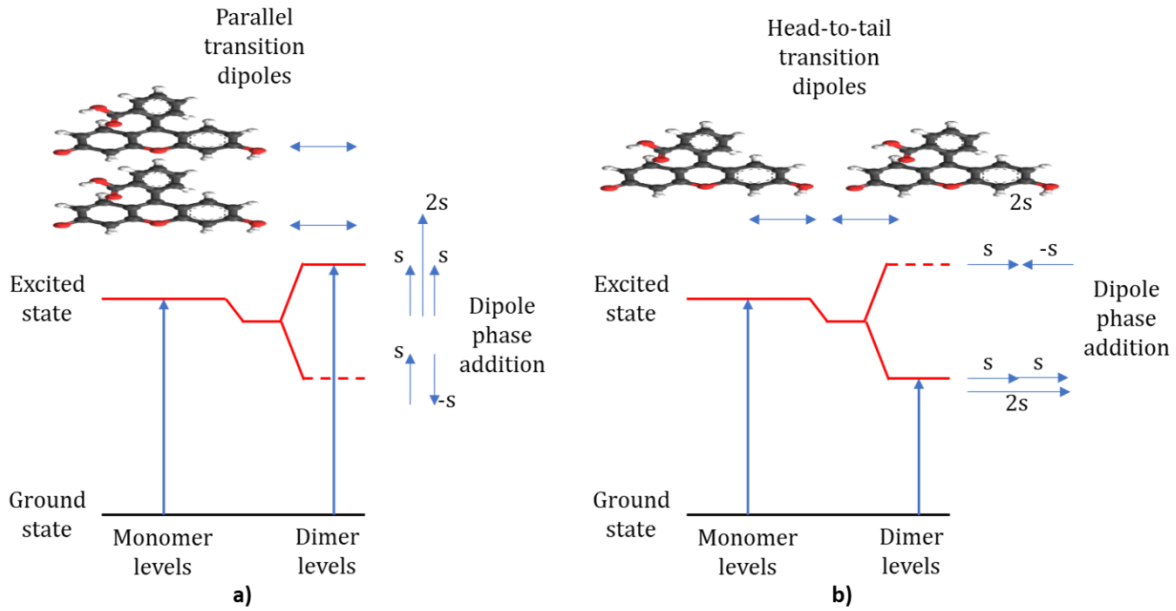

Figure 4 : Exciton band energy diagram for a molecular dimer with parallel (a) and head-to-tail (b) transition dipoles

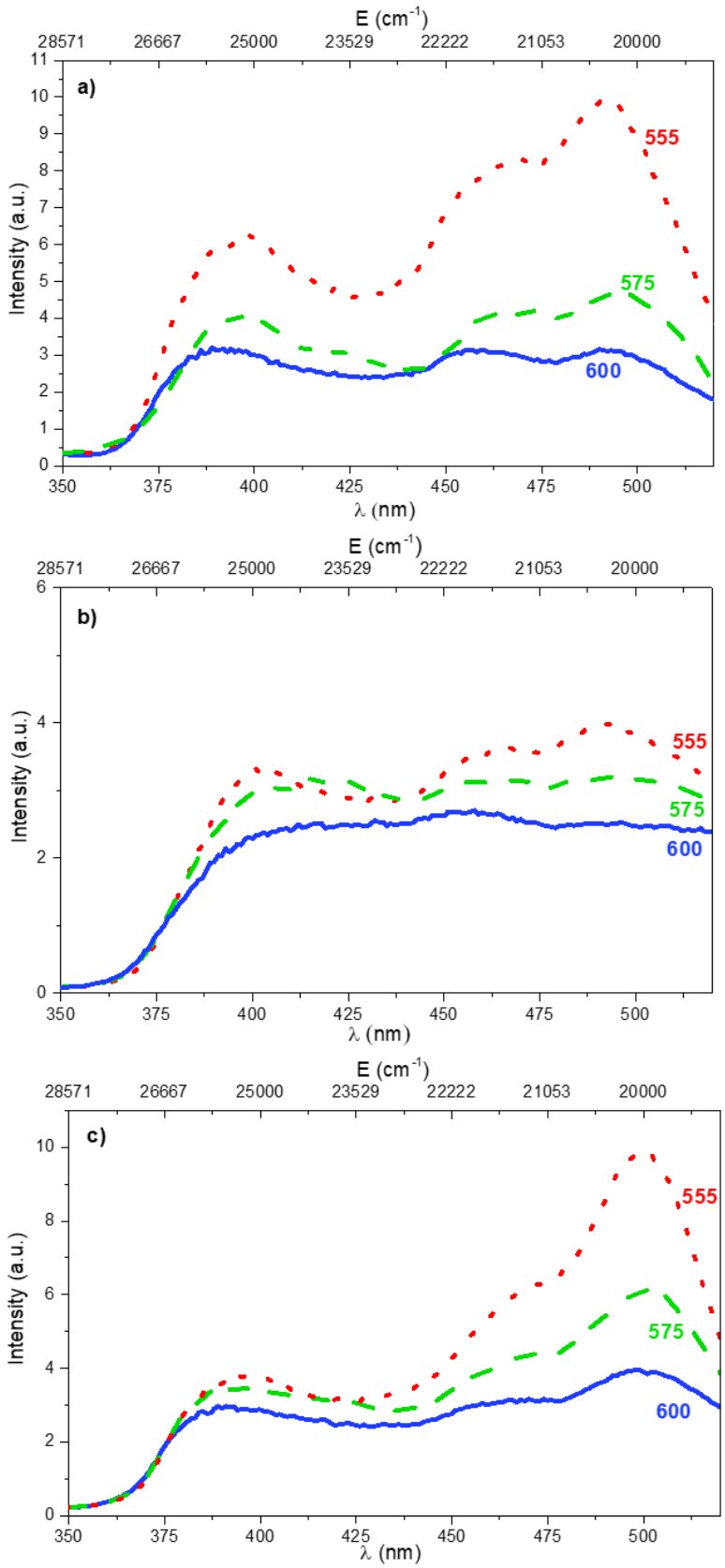

Figure 5 : Fluorescence excitation spectra monitoring at several wavelengths emission (555, 575 and 600) of: a) LDH-fluorescein (0,05%) powder b) calcinated LDH-nitrate with fluorescein adsorption c) LDH-carbonate with adsorbed fluorescein

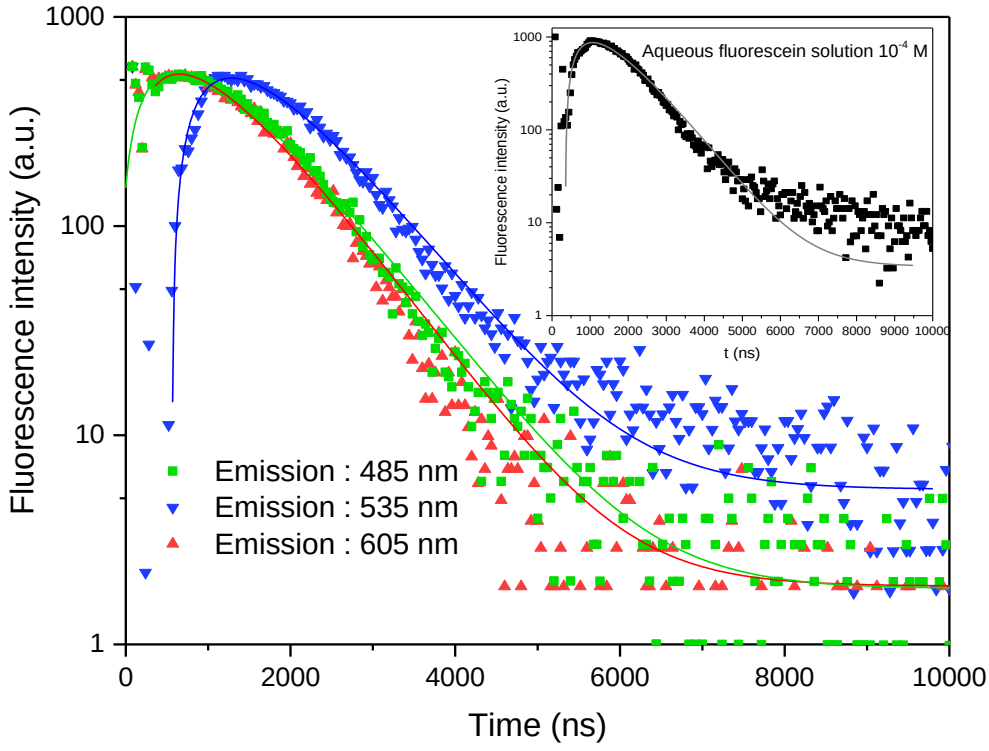

Figure 6: Fluorescence lifetime decay of the powder LDH-F (0.05%) monitored at different emission wavelengths and with an excitation wavelength fixed at 492 nm. Inset: fluorescence lifetime decay of aqueous fluorescein solution (10^{-4} M) with excitation wavelength fixed at 450 nm and emission wavelength at 520 nm.

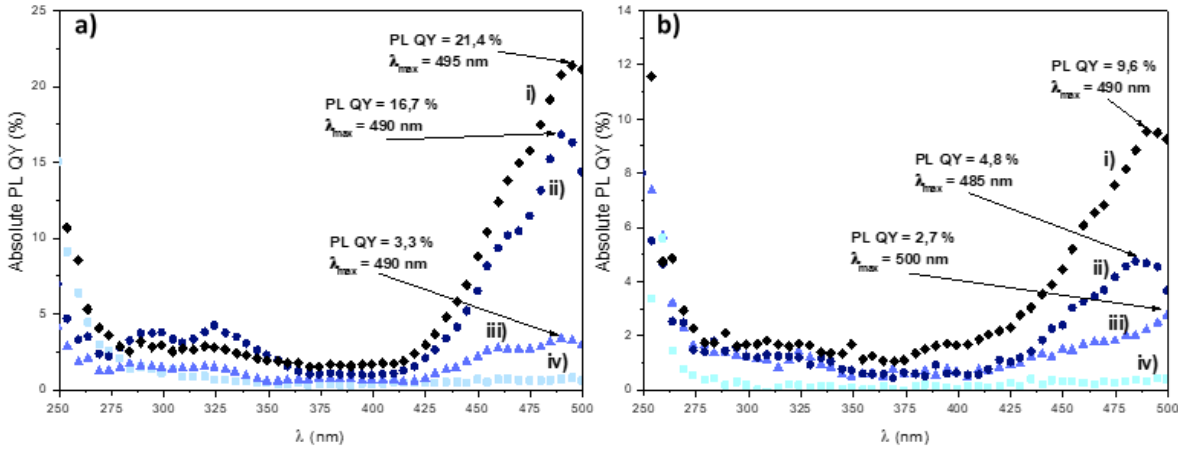

Figure 7: Absolute quantum yield depending on the wavelength with different amounts of fluorescein (i :0.05 %, ii: 0.1 %, iii: 1.25 %, iv: 10 for paste samples (a) and powder samples (b)

664

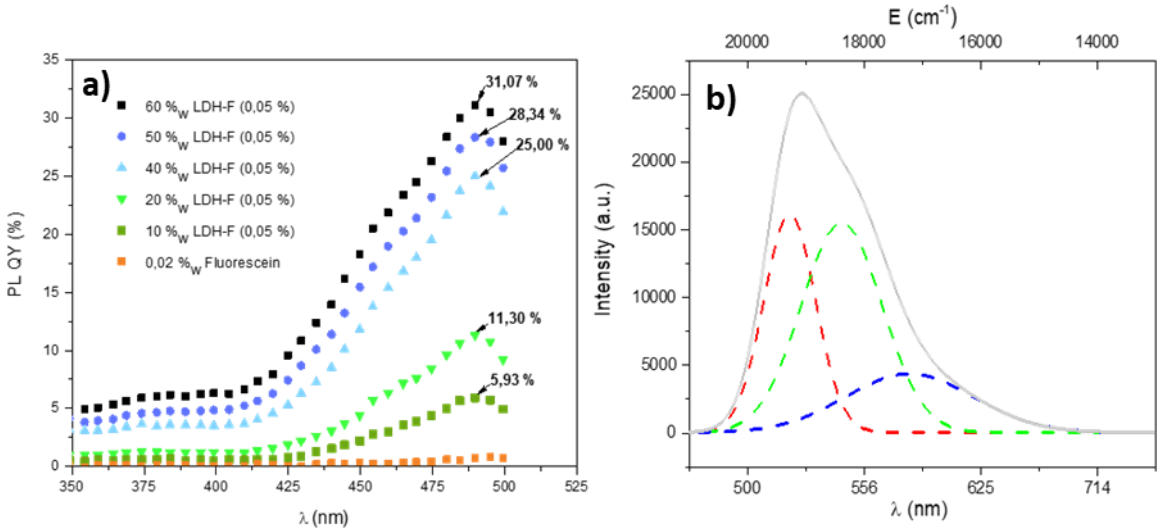

665

666 *Figure 8 : Absolute PL QY of composite films silicone/LDH-F (0,5 %) for several loadings of LDH powder (a). Emission*
667 *spectrum of a composite film silicone/LDH-F (0,05 %) 80:20 with λexc=450 nm (b).*

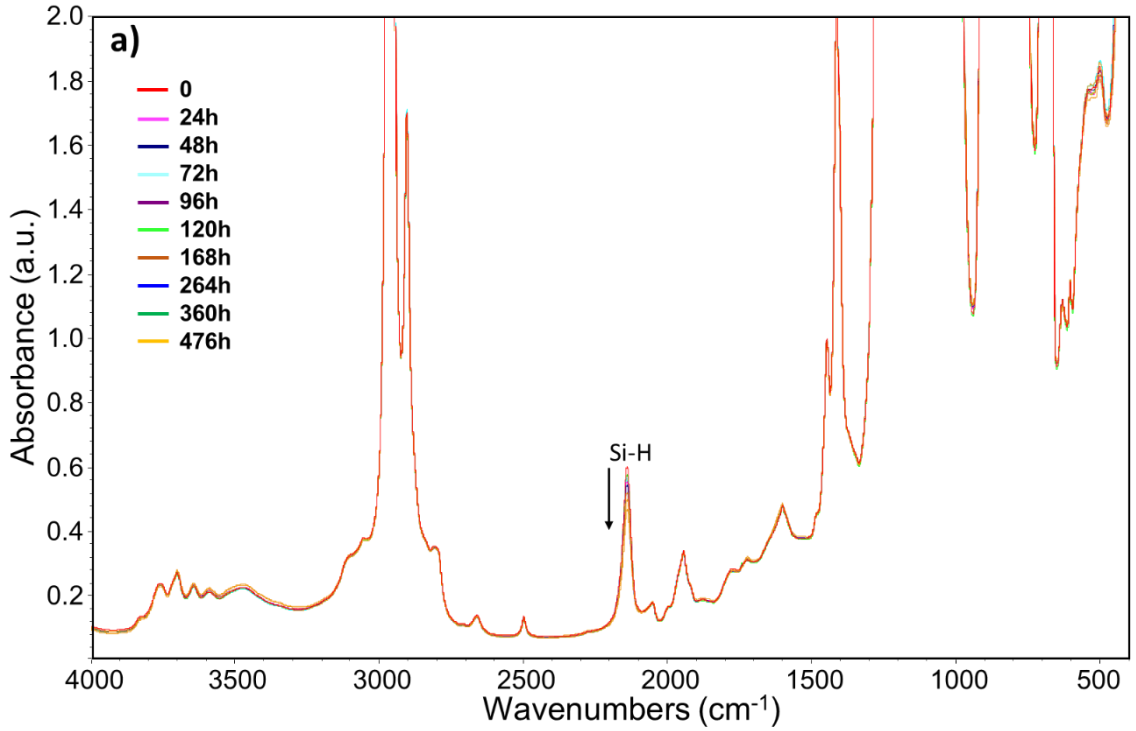

668

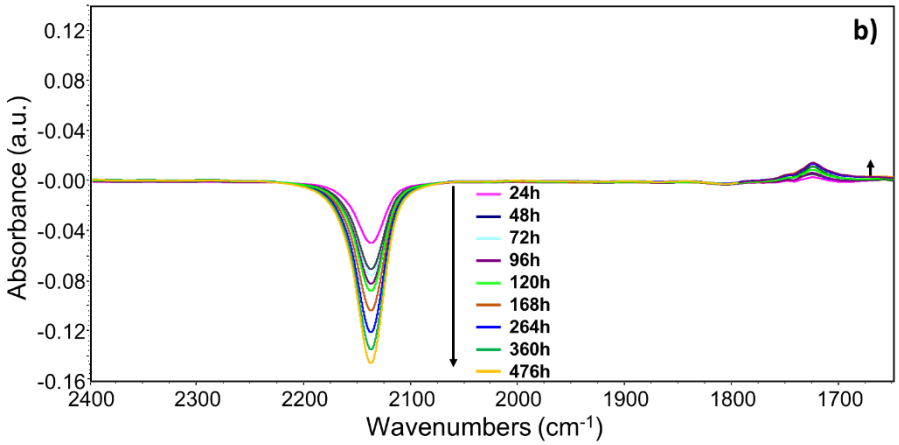

669

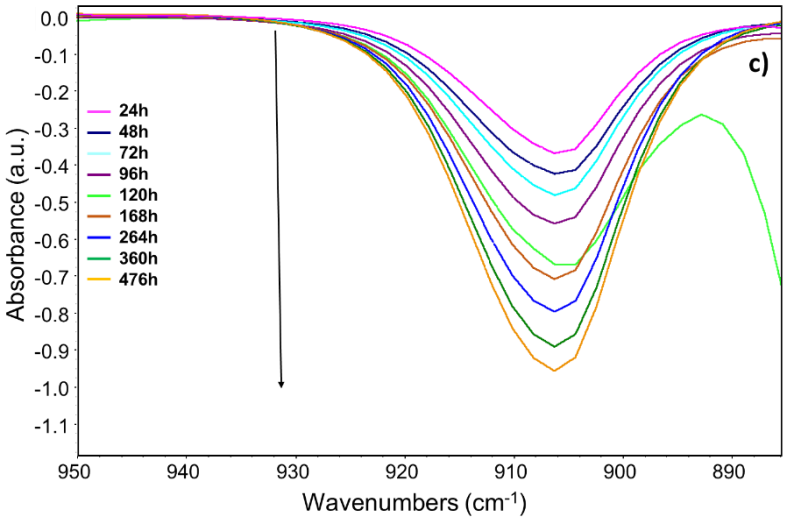

670
671 *Figure 9 : FTIR spectra during photooxidation at λ>300 nm, 60°C, of a pristine silicone film : a) between 400 and 4000 cm^{-1} b)*
672 *between 1650 and 2400 cm^{-1} (after subtraction of the initial spectrum) and c) between 885 and 950 cm^{-1} (after subtraction*
673 *of the initial spectrum).*

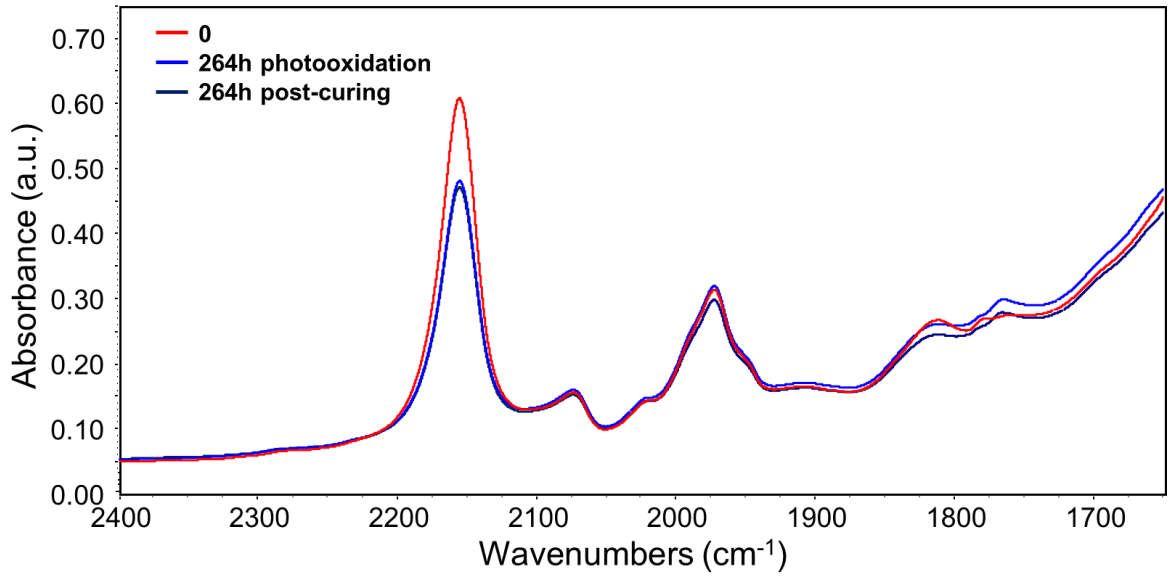

Figure 10 : FTIR spectra of a pristine silicone film (between 1600 and 2400 cm^{-1}), after 264h of photooxidation λ>300 nm, 60°C and after post-curing treatment in oven at 80°C.

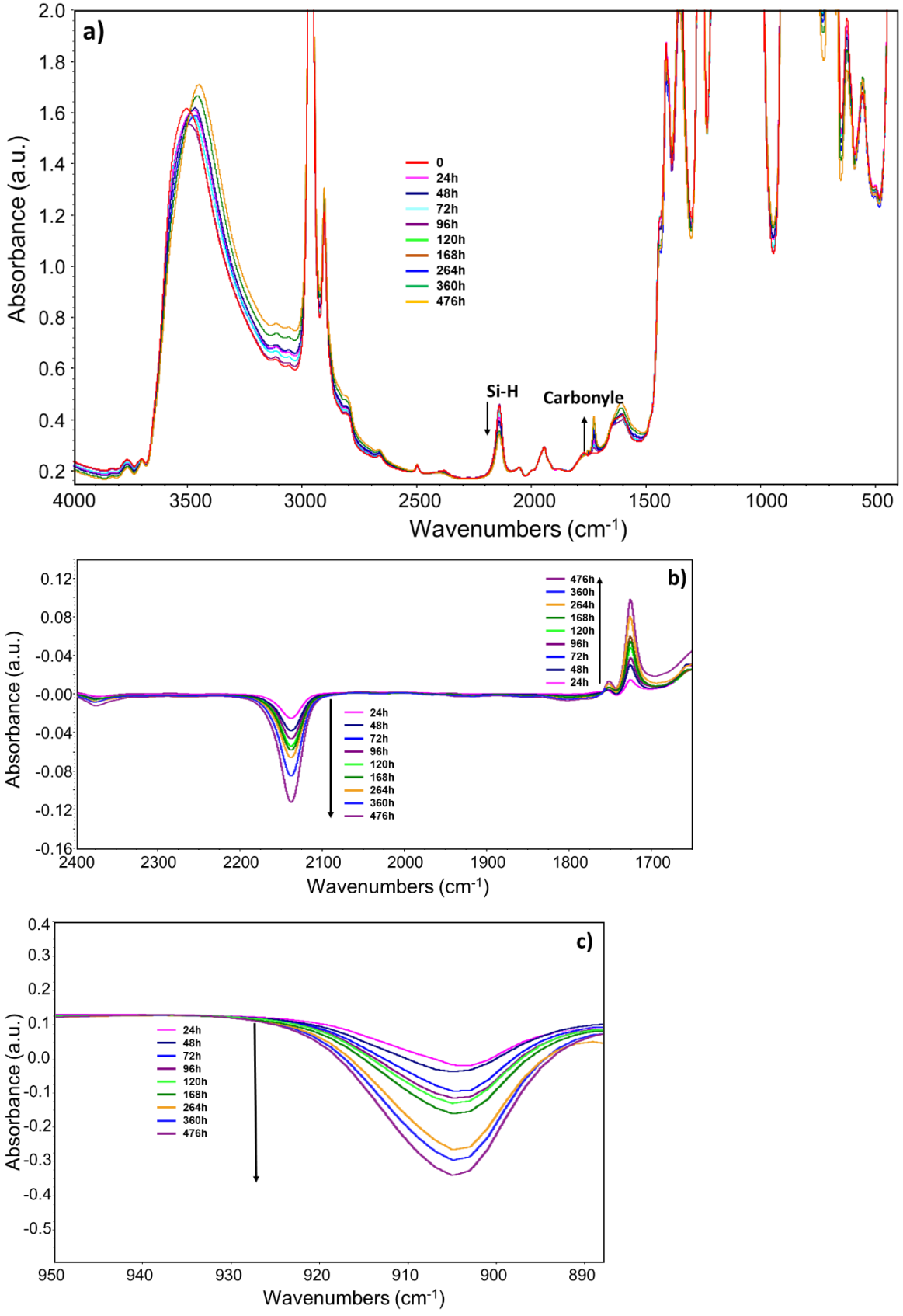

Figure 11: FTIR spectra during photooxidation at λ>300 nm, 60°C, of a composite film silicone/LDH-F (0.05%) (with 20 %w of LDH-F) : a) between 400 and 4000 cm^{-1} b) between 1650 and 2400 cm^{-1} (after subtraction of the initial spectrum) and c) between 885 and 950 cm^{-1} (after subtraction of the initial spectrum).

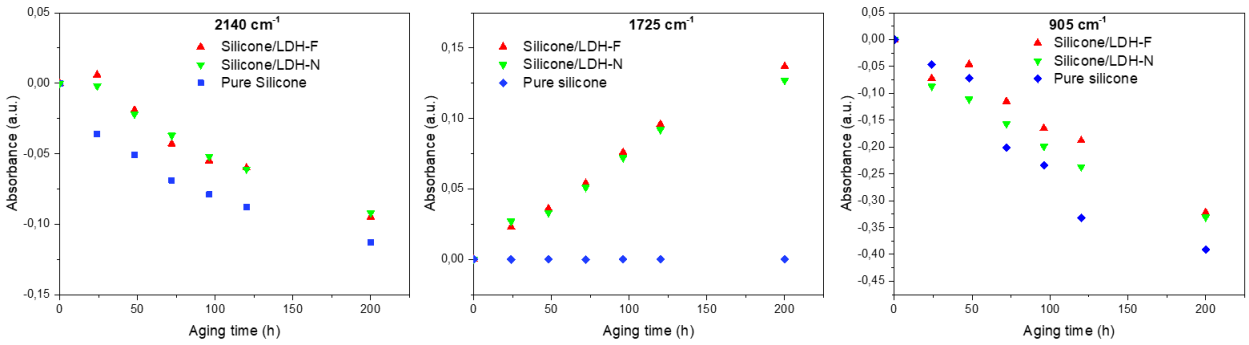

Figure 12: Variations of absorbance at 2140, 1725 and 905 cm^{-1} as a function of irradiation time for the composite film silicone/LDH-F (0.05%), the composite film silicone/LDH-N and the pristine silicone film

Supporting Information

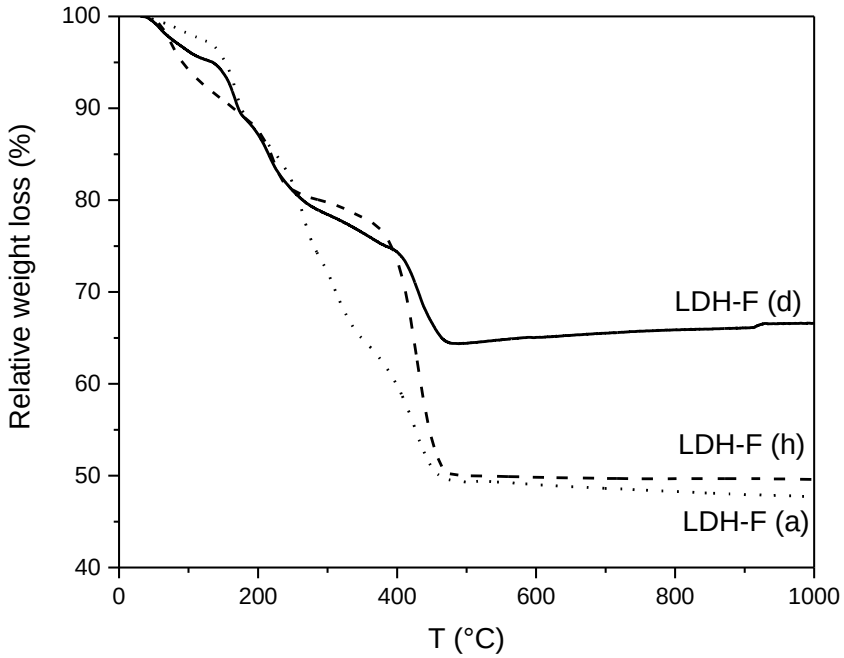

Figure S1: TGA of LDH-F powders under air (sample a, d and h)

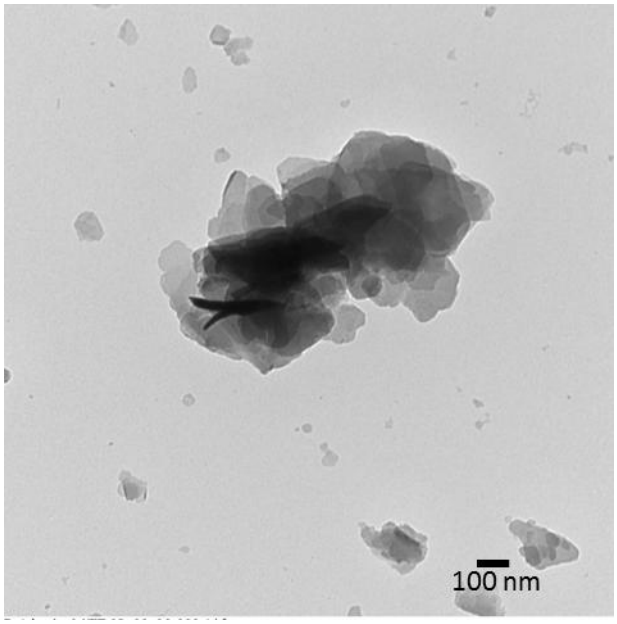

Figure S2: TEM image of LDH-F powder

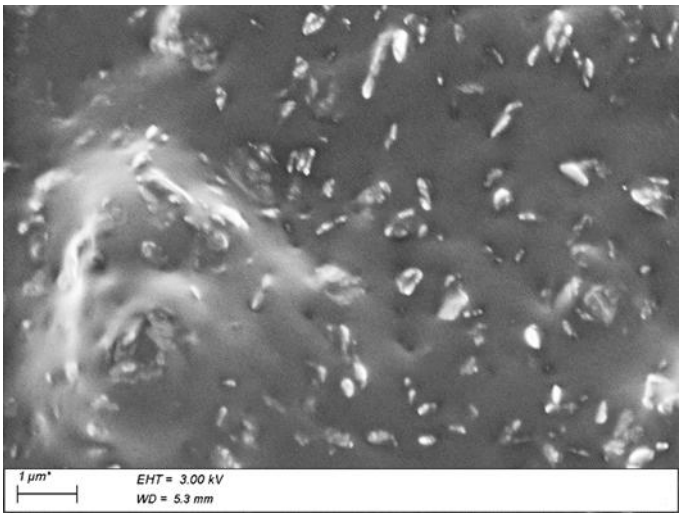

Figure S3: SEM image of Silicone/LDH-F composite film